



Facile synthesis of tremelliform $\text{Co}_{0.85}\text{Se}$ nanosheets: An efficient catalyst for the decomposition of hydrazine hydrate

Cheng-Cheng Liu^a, Ji-Ming Song^{a,*}, Jing-Feng Zhao^a, Hua-Jun Li^a, Hai-Sheng Qian^b, He-Lin Niu^a, Chang-Jie Mao^a, Sheng-Yi Zhang^a, Yu-Hua Shen^a

^a School of Chemistry and Chemical Engineering, Key Laboratory of Functional Inorganic Materials Chemistry of Anhui Province, Anhui University, Hefei, Anhui, 230039, PR China

^b Department of Chemistry, College of Chemistry and Life Sciences, Zhejiang Normal University, Jinhua, 321004, PR China

ARTICLE INFO

Article history:

Received 22 October 2011

Received in revised form 25 February 2012

Accepted 28 February 2012

Available online 6 March 2012

Keywords:

Tremelliform

Cobalt selenide

Catalytic decomposition

Hydrazine hydrate

Hydrazine compounds

ABSTRACT

Tremelliform $\text{Co}_{0.85}\text{Se}$ nanosheets have been successfully synthesized through a hydrothermal reaction of $\text{Co}(\text{NO}_3)_2 \cdot 6\text{H}_2\text{O}$, Na_2SeO_3 and $\text{N}_2\text{H}_4 \cdot \text{H}_2\text{O}$ without using any surfactant or structure-directing agents. The hydrothermal reaction products were confirmed as pure phase of $\text{Co}_{0.85}\text{Se}$. Scanning electron microscopy (SEM) and transmission electron microscopy (TEM) characterizations further showed that the obtained products were flexible tremelliform nanosheets, which were composed of the slices with thickness of ca. 10 nm. Additionally, detailed investigation indicated that the formation of the tremelliform $\text{Co}_{0.85}\text{Se}$ nanosheets was strongly dependent on the reaction temperature, reaction time and reactant ratios. The obtained tremelliform $\text{Co}_{0.85}\text{Se}$ nanosheets displayed ferromagnetic properties at room temperature according to the magnetic measurement. More interesting, the as-prepared $\text{Co}_{0.85}\text{Se}$ nanosheets showed efficient catalytic performance for decomposition of hydrazine hydrate at room temperature. In addition, the stability and reversibility of $\text{Co}_{0.85}\text{Se}$ nanosheets as catalysts are also excellent, indicating that these nanomaterials can be used as long term catalysts in wastewater treatment.

© 2012 Elsevier B.V. All rights reserved.

1. Introduction

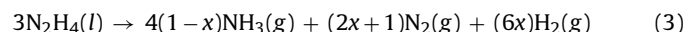
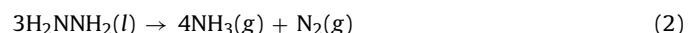
During the past few decades, much effort has been focused on the design of rational methods to synthesize metal chalcogenide nanomaterials with specific sizes, morphologies, and structures due to their potential applications in electronics, biochemical sensors, catalysis and to name a few [1–6]. As an important metal chalcogenide, cobalt selenide is known as a metallic conductor and exchange-enhanced Pauli paramagnet in its ground state with a Curie temperature (T_c) of 124 K [7,8]. Usually, there are three homogeneous and stable phases at room temperature (CoSe_2 , CoSe and $\text{Co}_{0.85}\text{Se}$) and two other possible compositions (Co_3Se_4 and Co_2Se_3) for cobalt selenides [9–13]. Cobalt selenide nanosheets have been prepared by several methods such as solvothermal [11,13], hydrothermal [10], mechanical alloying [14], microwave-assisted polyol process [15], and electrodeposition by potentiostatic route [16]. Zhan et al. [11] and Zhao et al. [13] reported the synthesis of nonstoichiometric cobalt selenide nanocrystals by a solvothermal reaction. Liu et al. synthesized urchin-like $\text{Co}_{0.85}\text{Se}$ nanocrystals via a hydrothermal reduction route [10]. According to literatures, cobalt selenides have mainly been applied as catalyst for the

oxygen reduction reaction [12,15,17,18]. However, to date, synthesis of the nonstoichiometric cobalt selenide ($\text{Co}_{0.85}\text{Se}$) and their efficiency for catalytic decomposition of hydrazine hydrate have rarely been researched.

Hydrazine has found various applications in many industrial, agricultural and other fields, including foaming and anticorrosive agents, synthetic resins, rubber additive, pharmaceuticals, and agricultural chemicals [19,20]. Besides being reactive and explosive, hydrazine is highly toxic. Inhalation results in eye and respiratory tract irritation with lung congestion, bronchitis and pulmonary edema [20]. In addition, hydrazine is suspected to be carcinogen [21]. Considering these high toxicological effects and its industrial significance, it is of great importance for completely removing hydrazine in the water using a suitable catalyst. There are different pathways for the decomposition of hydrazine, which depend on the catalyst used and the reaction conditions [22]. Recent studies, mostly on the reactions of hydrazine highly diluted in inert gases such as argon, have shown that hydrazine can be decomposed in two ways [23,24]: complete decomposition,



and incomplete decomposition,



* Corresponding author.

E-mail address: jiming@ahu.edu.cn (J.-M. Song).

As shown in Eqs. (1) and (2), there are two typical reaction routes for hydrazine decomposition. Eq. (3) describes the overall reaction of hydrazine decomposition. At present, the catalysts of hydrazine decomposition include carbides [25], nitrides [26], metals [23,27], alloys [28,29], ternary phosphides [30], and so on. One of the best commercial catalysts for hydrazine decomposition is the Ir/Al₂O₃ (20–40 wt% Ir) catalyst [26]. However, iridium is very rare and expensive. Hence, much effort should be devoted to developing catalysts with low cost.

Herein we report the synthesis of nonstoichiometric tremelliform Co_{0.85}Se nanosheets via a facile hydrothermal co-reduction route. The structure and morphology of the product have been discussed. Specific surface area and magnetic properties have also been studied. The catalytic property of the as-prepared samples has been further investigated by decomposition of hydrazine hydrate. The prepared Co_{0.85}Se nanosheets can be a potential substitute as catalyst for decomposition of hydrazine hydrate due to its high catalytic activity and reversibility.

2. Experimental details

2.1. Chemicals

All chemicals are of analytical grade and used as received, without further purification.

2.2. Synthesis of tremelliform Co_{0.85}Se nanosheets

The tremelliform Co_{0.85}Se nanosheets were synthesized through a hydrothermal route. In a typical procedure, Co(NO₃)₂·6H₂O (0.5 mmol) and Na₂SeO₃ (0.5 mmol) were respectively added into Teflon-lined stainless steel autoclave of 25 mL capacity. Subsequently, distilled water (18 mL) and N₂H₄·H₂O (2 mL, 85%) were added into the autoclave under vigorous stirring. The solution was stirred vigorously for 20 min and sealed. The autoclave was maintained at 140 °C for 24 h and then cooled to room temperature naturally. A black product was collected by centrifugation and washed with absolute ethanol and distilled water in sequence for several times. The final product was dried under vacuum at 60 °C for 4 h for further characterization.

2.3. Characterization

The phase purity and the crystallinity of the sample were characterized by powder X-ray diffraction (XRD, Rigaku D/max-RA, graphite monochromatized CuKα1 radiation, $\lambda = 0.15406$ nm). Scanning electron microscopy (SEM, S4800, Hitachi, Japan, at 5.0 kV), transmission electron microscopy (TEM, JEM-2100, JEOL, Japan, at 200 kV) and high resolution TEM (HRTEM) were used to characterize the morphologies and structures of samples. Nitrogen adsorption and desorption isotherms were measured at 77 K using a Micromeritics ASAP2020M+ C system after the samples were first degassed at 130 °C overnight. Specific surface areas were determined by the BET method and the mesopore size distribution was determined by the Barrett–Joyner–Halenda (BJH) method. For the BJH analysis, the pore size distribution was obtained from the analysis of the adsorption branch of the isotherm. Magnetic hysteresis loops were measured on a vibrating sample magnetometer (BHV-55) at room temperature. Inductively coupled plasma (ICP-OES, IRIS Intrepid II, Thermo Electron, USA) was used to determine the elemental composition of the samples. UV-vis spectroscopic measurements of the samples were carried out with a UV-3600 model UV-vis double beam spectrophotometer (Japan Shimadzu Co.) operated at a resolution of 2 nm.

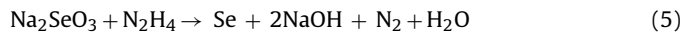
2.4. Measurement of catalytic activity

The evaluation of catalytic activity of the prepared products for decomposition of hydrazine hydrate was performed at 25 °C. The concentration of hydrazine in the working solution was determined via the modified method reported in previous literature [31]. The color reagent employed has the following composition: p-dimethylaminobenzaldehyde, 8 g; ethanol, 50.0 mL; concentrated hydrochloric acid, 50.0 mL. In order to determine the best concentration of hydrazine in this color development experiment, we plotted a standard curve. The details were as follows: we transferred different volume of 2.0×10^{-3} M of the hydrazine hydrate solutions to a 50 mL beaker with 2.5 mL color reagent and some distilled water (the total volume of the solution maintained at 25 mL), and then the mixture was kept at room temperature for 10 min to form hydrazone mixture solution. The concentration of hydrazine was determined by hydrazone mixture solution on the UV-vis spectrophotometer. To examine the stability of hydrazine hydrate, 100 mL 2.0×10^{-3} M of the hydrazine hydrate solution was placed for several days at room temperature in the absence of the catalysts. The results showed that the hydrazine hydrate was not decomposed. In our catalysis experiments, 50 mg Co_{0.85}Se catalyst was added into a 250 mL round bottom flask with 100 mL of 2.0×10^{-3} M hydrazine hydrate solution, then the mixture was stirred strongly with a magnetic stirrer and kept at 25 °C in a water bath to ensure a homogeneous temperature distribution during the hydrazine decomposition. We took 5 mL of the mixture to centrifuge at different time intervals, then transferred 0.5 mL supernatant liquid to a 50 mL beaker with 2.5 mL color reagent and 22.0 mL distilled water and then placed the solution for 10 min at ambient condition. The above solution was further determined on the UV-vis spectrophotometer. Cycle experiments were as follows: first, 200 mg Co_{0.85}Se catalyst was put into 400 mL of 2.0×10^{-3} M hydrazine hydrate solution in a glassware, and then the mixture was stirred strongly with a magnetic stirrer at 25 °C. We took 5 mL of the mixture at different intervals (10, 20, 30, 40, 50 and 60 min) to centrifuge, and then transferred 0.5 mL of the supernatant liquid for further measurement of the concentration of the hydrazine hydrate. The catalysts used once were collected by centrifugation and washed with absolute ethanol and distilled water in sequence for several times, then dried under vacuum at 60 °C for 4 h. The following five repeated experiments for testing the stability of the products were the same as the above procedures. It was notable that Co_{0.85}Se catalyst would suffer loss during the centrifugal washing. Therefore, to ensure the accuracy of the experiment, we kept the ratio of 50 mg Co_{0.85}Se catalyst corresponding to 100 mL of 2.0×10^{-3} M hydrazine hydrate solution in each test.

3. Results and discussion

3.1. Morphology and structure

High-yield synthesis of tremelliform single-crystalline Co_{0.85}Se nanosheets have been realized for the first time via a facile hydrothermal approach by reducing Co(NO₃)₂·6H₂O and Na₂SeO₃ with N₂H₄·H₂O. The chemical reactions can be expressed as the following equations [32,33]:



Firstly, N₂H₄ can reduce Co²⁺ and SeO₃²⁻ into elemental Co and Se, respectively. Then Co reacts with Se to form cobalt selenide nanocrystalline with tremelliform structure. The

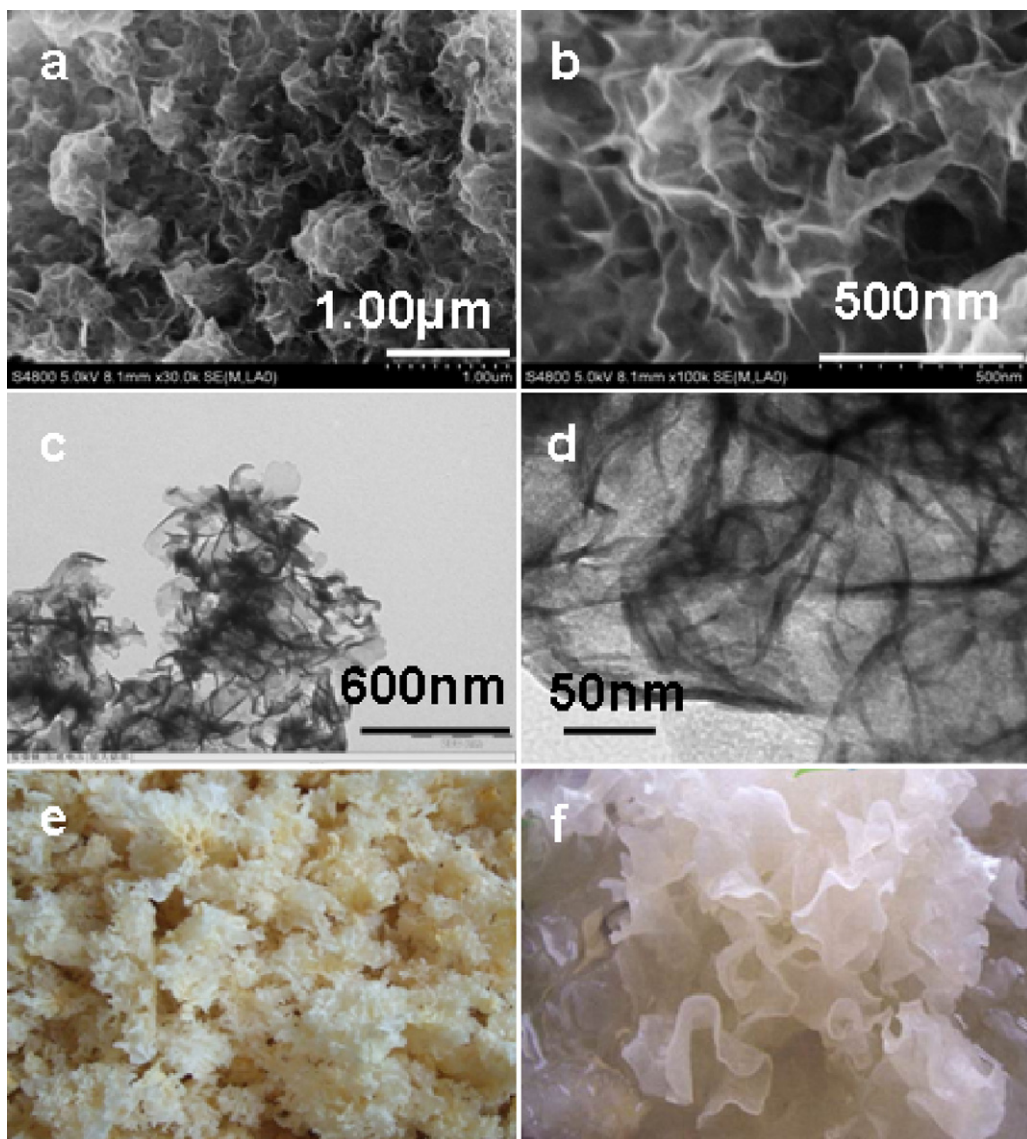


Fig. 1. SEM images (a and b) and TEM images (c and d) of tremelliform $\text{Co}_{0.85}\text{Se}$ and the actual tremella photos (e and f). (a and c) at a low magnification; (b and d) at high magnification.

low-magnification image (Fig. 1a) reveals that the products have a tremelliform structure. SEM image in high magnification (Fig. 1b) clearly exhibits the actual morphology of $\text{Co}_{0.85}\text{Se}$ products is thin and slippery slices with thickness of ca. 10 nm, which is similar to graphene-like $\text{Co}_{0.85}\text{Se}$ nanocrystallines prepared via solvothermal route [13]. The morphology of the as-prepared products is like natural tremella by comparing SEM images (Fig. 1a and b) with the actual tremella photos (Fig. 1e and f). TEM image (Fig. 1c) shows the morphology of the prepared $\text{Co}_{0.85}\text{Se}$ nanosheets is also thin and uniform, which is in good agreement with the SEM images and the high-magnification TEM image (Fig. 1d).

Fig. 2 shows the typical X-ray diffraction (XRD) pattern for the as-prepared $\text{Co}_{0.85}\text{Se}$ nanosheets. All diffraction peaks can be indexed to the phase of $\text{Co}_{0.85}\text{Se}$ hexagonal structure, which match well with the standard data file of $\text{Co}_{0.85}\text{Se}$ (JCPDS file No. 52-1008). No peaks from other phases can be detected. The three strongest peaks of $\text{Co}_{0.85}\text{Se}$, at $2\theta = 33.3^\circ$, 45.1° and 51.1° are assigned to the (101), (102) and (110) planes of the hexagonal close-packed (hcp) $\text{Co}_{0.85}\text{Se}$ [space group: $P6_3/mmc$ (194)]. The selected area electron diffraction pattern (SAED, Fig. 3a) shows the single $\text{Co}_{0.85}\text{Se}$ nanosheet is single-crystalline structure according to the

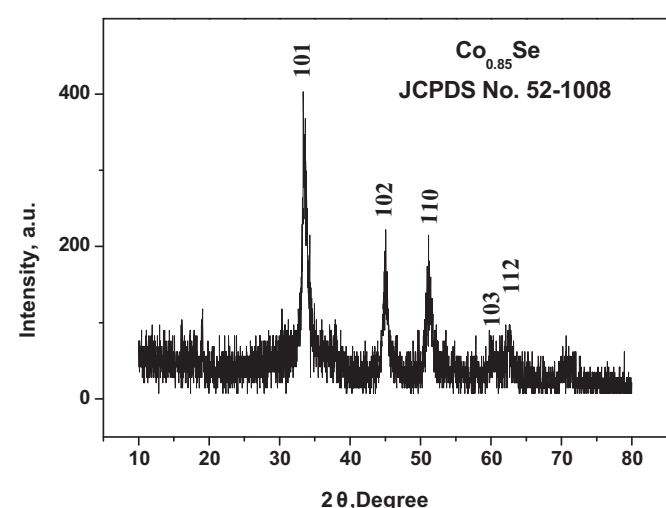


Fig. 2. XRD pattern of the obtained $\text{Co}_{0.85}\text{Se}$ nanosheets.

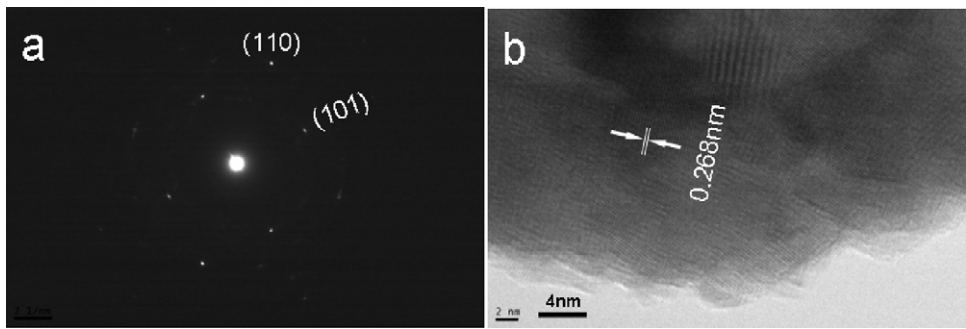


Fig. 3. (a) SAED pattern of a single tremelliform $\text{Co}_{0.85}\text{Se}$ nanosheet. (b) HRTEM image of the designated $\text{Co}_{0.85}\text{Se}$ nanosheet.

diffraction spots from the (110) and (101) Bragg reflections of hexagonal close-packed (hcp) cobalt selenide. The tremelliform $\text{Co}_{0.85}\text{Se}$ is further investigated by the HRTEM analysis (Fig. 3b). Clear and continuous lattice fringe can be observed. The distance between neighboring fringes is measured to be 0.268 nm, close to the (101) lattice spacing of $\text{Co}_{0.85}\text{Se}$. The obtained cobalt selenide has a NiAs structure, in which the cobalt and selenium are both six-coordinate. Even though the cobalt and selenium have the same coordination number, they do not have the same coordination environment in the NiAs structure. The selenium atoms have a hexagonal close-packed arrangement, and the cobalt atoms occupy the octahedral interstitial sites with the tetrahedral sites empty. The selenium atoms have six cobalt neighbors arranged as a trigonal prism. It is a characteristic feature for this structure to show a variable composition [11].

3.2. Magnetic properties and nitrogen sorption analysis

Magnetic measurements on the prepared tremelliform $\text{Co}_{0.85}\text{Se}$ nanosheets have been conducted. The M–H hysteresis loop measured at room temperature is presented in Fig. 4, which shows coercivity (H_c), saturation magnetization (M_s) and remanent magnetization (M_r) values of ca. 331.4 Oe, 0.0117 and 0.0907 emu/g, respectively. The M–H curve indicates that the tremelliform $\text{Co}_{0.85}\text{Se}$ nanosheets have weak ferromagnetism. Compared with the H_c value of the graphene-like $\text{Co}_{0.85}\text{Se}$ nanocrystallines (263 Oe) [13], that of cobalt selenide nanosheets prepared in present condition was enhanced.

Brunauer–Emmett–Teller (BET) gas sorptometry measurements have been conducted to examine the tremelliform $\text{Co}_{0.85}\text{Se}$

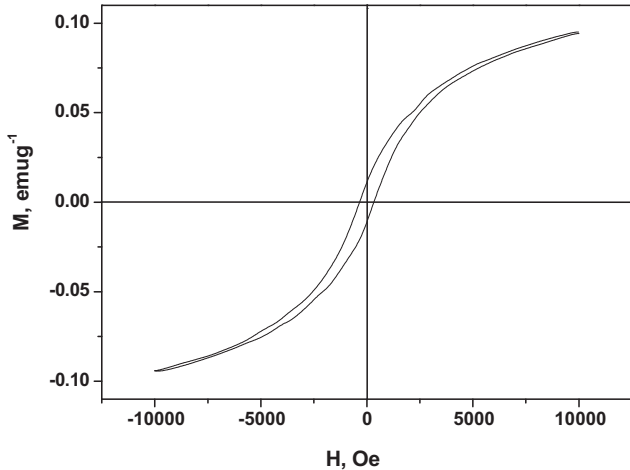


Fig. 4. Magnetic hysteresis loop for as-obtained $\text{Co}_{0.85}\text{Se}$ nanosheets at room temperature.

nanosheets. Fig. 5 shows the N_2 adsorption/desorption isotherm and the pore-size distribution (inset) of the tremelliform $\text{Co}_{0.85}\text{Se}$. The isotherm can be categorized as type IV with a distinct hysteresis loop observed in the range of $0.45\text{--}1.0 \text{ } p/p_0$, which is characteristic of mesoporous materials. BET specific surface area of the synthesized sample is calculated from N_2 isotherms at 77.5 K and is found to be $55.1 \text{ m}^2 \text{ g}^{-1}$, and this value is higher than that of graphene-like $\text{Co}_{0.85}\text{Se}$ nanocrystallines ($12.6 \text{ m}^2 \text{ g}^{-1}$) reported previously [13]. The pores of around 45 nm are attributed to the interparticle spaces, determined by using the Barrett–Joyner–Halenda (BJH) method (inset in Fig. 5). The high BET surface area of the catalyst would provide more active sites for the catalytic reaction.

3.3. Influence of reaction conditions

The influence of temperature for the prepared $\text{Co}_{0.85}\text{Se}$ has been investigated. The XRD patterns of the samples prepared at different reaction temperature are shown in Fig. S1. When the temperature changed from 80°C to 120°C , the cobalt selenide had a lower crystallinity comparing with the products prepared at 140°C (Fig. S1a–c). The products were a mixture of $\text{Co}(\text{OH})_2$ (JCPDS file No. 30-0443) and $\text{Co}_{0.85}\text{Se}$ (Fig. S1d and e), when the temperature exceeded 160°C . Fig. S2 shows the SEM images of the samples prepared at different temperature. The SEM images reveal that the products had an obvious non-uniform netlike structure with a little agglomeration, when the temperature was at 100°C or 120°C (Fig. S2a and b). If the temperature was at 160°C , the flexible thin sheet structures were damaged, while at 180°C , the products had a seriously agglomerated shape (Fig. S2c and d). So the most suitable

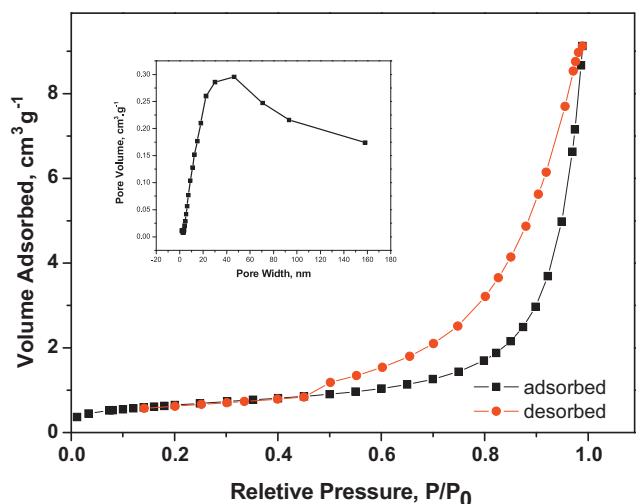


Fig. 5. Nitrogen adsorption/desorption isotherm and Barrett–Joyner–Halenda (BJH) pore size distribution plot (inset) of the tremelliform $\text{Co}_{0.85}\text{Se}$ nanosheets.

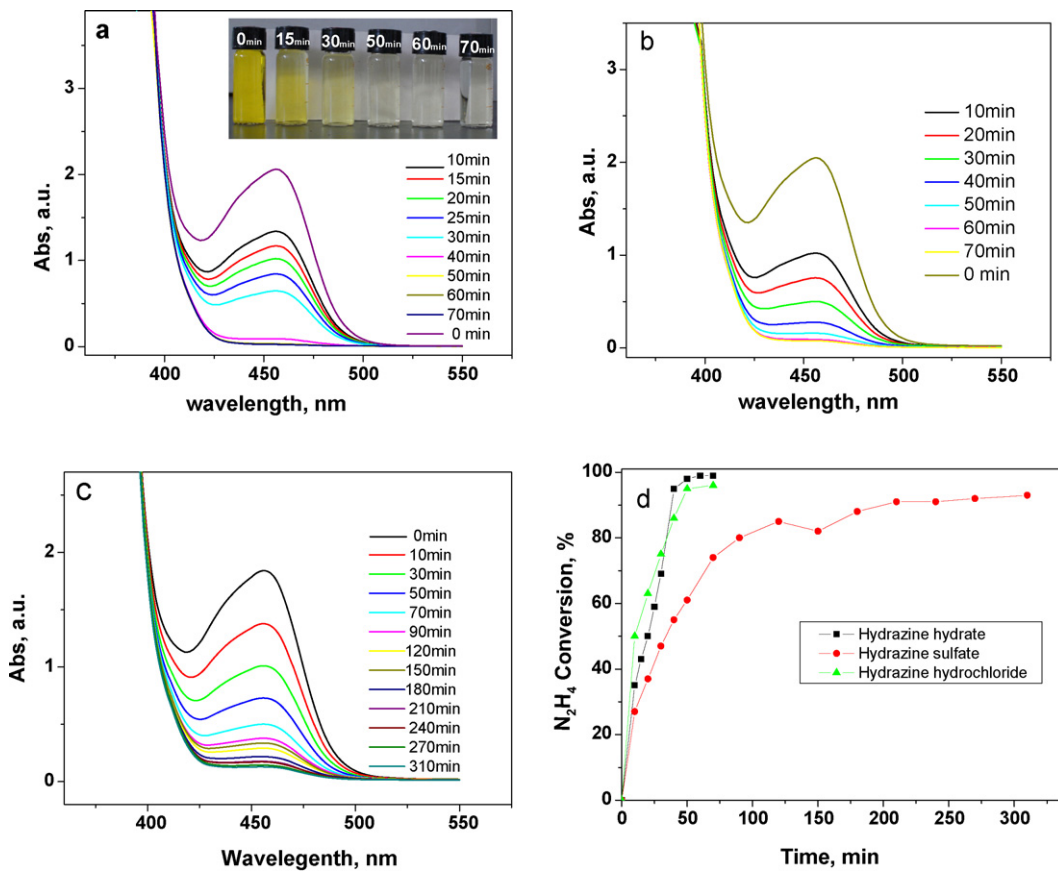


Fig. 6. UV-vis absorption spectra for the process of the decomposition of (a) hydrazine hydrate; (b) hydrazine hydrochloride; (c) hydrazine sulfate; (d) the conversion rates of hydrazine hydrate, hydrazine hydrochloride and hydrazine sulfate over the Co_{0.85}Se nanosheet catalysts.

temperature is 140 °C for the synthesis of uniform thin Co_{0.85}Se nanosheet, and this temperature is lower than that of graphene-like Co_{0.85}Se nanocrystallines prepared previously (180 °C) [13].

The influences of the different volume of hydrazine hydrate and the different mole ratios of Co(NO₃)₂·6H₂O to Na₂SeO₃ have also been examined. From the XRD patterns of the products prepared at different volume of hydrazine hydrate, we can see that the phases of the samples became impure if the volume of hydrazine hydrate was less than 1 mL in the present synthesis system (Fig. S3a and b). The widened XRD peak indicates that the crystallinity of Co_{0.85}Se nanosheets decreased with increasing the dosage of hydrazine hydrate (Fig. S3d and e). There are two main reasons for the result: (1) it is well known that quick reaction speed will lead to the decreasing of crystallinity of products. In our synthesis system, the reaction speed will increase while the dosage of hydrazine hydrate is added, resulting in the reduction of the crystallinity of Co_{0.85}Se nanosheets. (2) In addition, the decomposition of excessive hydrazine hydrate will produce a large number of bubbles in this system, and these bubbles also affect the growth and crystallization of Co_{0.85}Se nanocrystalline. SEM images clearly show that the products prepared by using 3 mL and 4 mL hydrazine hydrate, respectively, have a membrane structure (Fig. S4). The XRD patterns of the products prepared at different mole ratios (2:1 and 3:1) of Co(NO₃)₂·6H₂O to Na₂SeO₃ show that the phases of the samples also became impure by adding superfluous Co(NO₃)₂·6H₂O (Fig. S5). The solutions appear basic (pH 11.3, corresponding to the presence of 2 mL N₂H₄·H₂O) in our reaction system, and the superfluous Co²⁺ ions would turn into Co(OH)₂ in this alkaline conditions. However, the XRD pattern of the products prepared at 1:1 mole ratio of Co(NO₃)₂·6H₂O to Na₂SeO₃ shows that there was no the diffraction peak for Co(OH)₂ (Fig. S5c). This may be because

plentiful of NH₃ from the decomposition of hydrazine hydrate and the freshly formed Co(OH)₂ react into complex ion, [Co(NH₃)₆]²⁺, which could be removed in later washing. But if the amount of N₂H₄·H₂O is low or Co(NO₃)₂·6H₂O is superfluous, the complex ion does not completely form, in which case Co(OH)₂ would not be separated out from solution and still remain in the samples as residue. Therefore, the Co(OH)₂ would not be separated out from solution and still remained in the samples as residue (Fig. S3a and b, Fig. S5a and b). We can conclude that the phase of the products would remain pure by adding more than 2 mL N₂H₄·H₂O (85%) or less than 1 mmol Co(NO₃)₂·6H₂O under the other conditions remaining unchanged.

The influence of reaction time has been discussed. Figs. S6 and S7 show the SEM images and XRD patterns of the samples prepared at certain reaction time intervals. In this system the morphology of the products was strongly influenced by the reaction time while their phases almost did not change. It clearly shows that, after reaction for 6 h, some membrane structure appeared (Fig. S6a and b). After 12 h, the products had a uniform membrane structure (Fig. S6c and d). After 36 h, there were some small particles in the sample (Fig. S6e and f). By further elongating the reaction time to 48 h, more particles were formed (Fig. S6g and h), and TEM images display that the some of the particles were hollow spheres (inset in Fig. S6h). From the XRD patterns of the products prepared at different reaction time, it can be seen that the phase of all the samples was hexagonal phase of Co_{0.85}Se structure with cell constant $a = 3.165 \text{ \AA}$ and $c = 5.283 \text{ \AA}$ (Fig. S7). So, the proper reaction time is 24 h for obtaining thin and flexible uniform Co_{0.85}Se nanosheets. In addition, reaction time has a small influence on the phase of the sample, but a great influence on the morphology of the sample.

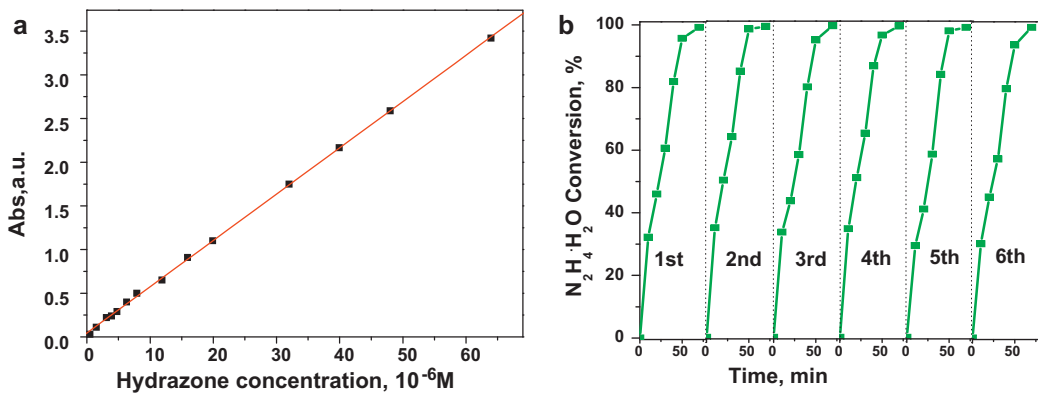


Fig. 7. (a) The standard curve of the absorbance of hydrazone vs. its concentrations; (b) the conversion curves of hydrazine hydrate over $\text{Co}_{0.85}\text{Se}$ nanosheets reused at different times.

3.4. Catalytic activity of tremelliform $\text{Co}_{0.85}\text{Se}$ nanosheets

In our case, we have found the obtained tremelliform $\text{Co}_{0.85}\text{Se}$ nanosheets have efficient catalytic activity for the decomposition of hydrazine hydrate. The evaluation of the catalytic activity for decomposition of hydrazine hydrate has been determined on the UV/vis spectrophotometer. The hydrazine hydrate undergoes condensation reaction with p-dimethylaminobenzaldehyde in acidic condition to form a yellow hydrazone, which has an absorption maximum at 456 nm in acidic condition. We protracted a standard curve by plotting the mean absorbance for each standard concentration (X axis) against the target hydrazone concentration (Y axis). A representative standard curve is shown in Fig. 7a, and it indicates a good linear relationship between the hydrazone absorbance and its concentration from 4.0×10^{-7} to 6.4×10^{-5} M. In order to keep the concentration of hydrazone within the linear range, we took 0.5 mL supernatant liquid of the mixture of $\text{Co}_{0.85}\text{Se}$ nanosheets and hydrazine hydrate at different time interval to react with color reagent, for further UV/vis absorption spectra test. UV/vis absorption spectra tests show that the absorbance of hydrazone at 456 nm dropped rapidly as the catalytic reaction time increased and disappeared almost completely within 60 min. The corresponding color of the hydrazone solution changed from yellow to nearly colorless (photos shown as inset in Fig. 6a). Catalytic activity of $\text{Co}_{0.85}\text{Se}$ nanosheets is shown in Fig. 6d. Hydrazine conversion rate over the catalyst rose up to 95% after 50 min. After catalytic reaction completing, the catalysts were collected by centrifugation without washing, and then were dispersed into 2.5 mL color reagent and 22.5 mL distilled water for 10 min (the total volume 25 mL, as solution 1). As reference, 2.5 mL color reagent was diluted to 25 mL, as solution 2. UV/vis absorption spectra showed that the

absorption of the solution 1 was the same as that of solution 2, which indicates that the removal of hydrazine hydrate was due to catalytic decomposition rather than adsorption. According to our experiments, 0.2 g $\text{N}_2\text{H}_4\text{-H}_2\text{O}$ can be completely decomposed by 1 g $\text{Co}_{0.85}\text{Se}$ nanosheets in 60 min at room temperature.

The prepared $\text{Co}_{0.85}\text{Se}$ nanosheets also had exhibited good performance on decomposition of other hydrazine compounds, such as hydrazine hydrochloride ($\text{N}_2\text{H}_4\text{-HCl}$) and hydrazine sulfate ($\text{N}_2\text{H}_4\text{-H}_2\text{SO}_4$). Fig. 6b and c showed that the decomposition of $\text{N}_2\text{H}_4\text{-HCl}$ and $\text{N}_2\text{H}_4\text{-H}_2\text{SO}_4$ in the presence of $\text{Co}_{0.85}\text{Se}$ nanosheets. Fig. 6d displays the conversion rate of $\text{N}_2\text{H}_4\text{-H}_2\text{O}$, $\text{N}_2\text{H}_4\text{-HCl}$ and $\text{N}_2\text{H}_4\text{-H}_2\text{SO}_4$ decomposed by $\text{Co}_{0.85}\text{Se}$ nanosheets. An almost complete decomposition of $\text{N}_2\text{H}_4\text{-HCl}$ was observed over $\text{Co}_{0.85}\text{Se}$ nanosheets after 70 min, while the conversion rate was only about 73.8% for $\text{N}_2\text{H}_4\text{-H}_2\text{SO}_4$ under similar condition, and the value reached 92% until 310 min. We can clearly see that the decomposition activity of $\text{Co}_{0.85}\text{Se}$ nanosheets on $\text{N}_2\text{H}_4\text{-HCl}$ is better than that of $\text{N}_2\text{H}_4\text{-H}_2\text{SO}_4$. Here, the acidity of the solution increase in the order of $\text{N}_2\text{H}_4\text{-H}_2\text{O} < \text{N}_2\text{H}_4\text{-HCl} < \text{N}_2\text{H}_4\text{-H}_2\text{SO}_4$. It has been reported that the rate of catalytic decomposition of hydrazine decreases with the increase of acidity, which is explained by the hydrogen ions competitive adsorption on the active catalyst centers [34].

In order to investigate the stability of the catalyst, repeatability experiments for the decomposition of hydrazine hydrate have been carried out in the same experiment conditions. The as-prepared $\text{Co}_{0.85}\text{Se}$ nanosheets show high catalytic stability during the catalytic reaction process and the conversion rates of $\text{N}_2\text{H}_4\text{-H}_2\text{O}$ all exceed 95% after 60 min (Fig. 7b). After the catalysts were recycled six times, the XRD and SEM of the sample were measured. From the XRD patterns and SEM images of the catalysts before and

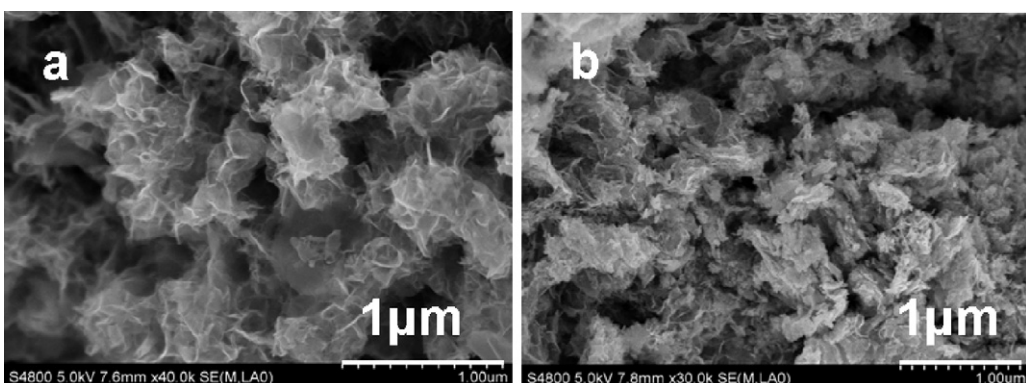


Fig. 8. (a) SEM of original $\text{Co}_{0.85}\text{Se}$ nanosheets; (b) SEM of $\text{Co}_{0.85}\text{Se}$ nanosheets reused six times.

after reaction, we can see that the phase of the samples did not change but the beautiful slice morphology was damaged to some extent, which may be because of the effect of external force, such as centrifugation, stirring, washing, and drying of the catalyst during the catalysts reused process (Fig. S8, Fig. 8). Except for little changes in the morphology, the present study shows that $\text{Co}_{0.85}\text{Se}$ nanosheets were not poisoned after they recycled more than six times for decomposition of hydrazine hydrate. So, the as-prepared $\text{Co}_{0.85}\text{Se}$ nanosheets are stable as a solid phase catalyst.

We also did the repeatability experiments for the decomposition of hydrazine hydrochloride and hydrazine sulfate. The results show that the $\text{Co}_{0.85}\text{Se}$ nanosheets could not be reused for decomposition of hydrazine hydrochloride and hydrazine sulfate. As we all know, hydrazine sulfate and hydrochloride are corrosive. In order to test the solubility of the catalysts in the presence of hydrazine sulfate and hydrazine hydrochloride, we have determined the metal content of the remaining solution after completion of the decomposition reaction by ICP tests. The results indicate the mass proportions of the dissolved catalyst in hydrazine sulfate and hydrazine hydrochloride solutions are 7.7% and 8.3%, respectively. So, some of the catalysts would be corroded in the presence of hydrazine sulfate and hydrazine hydrochloride. Therefore, $\text{Co}_{0.85}\text{Se}$ nanosheets have excellent catalytic activity and a good reusability for the decomposition of hydrazine hydrate, but they have poor reusability for the decomposition of hydrazine hydrochloride and hydrazine sulfate.

4. Conclusion

In summary, the synthesis of single-crystalline $\text{Co}_{0.85}\text{Se}$ with tremelliform morphology has been realized for the first time via a facile hydrothermal approach. The magnetic hysteresis loop measurement shows that the $\text{Co}_{0.85}\text{Se}$ nanosheets display ferromagnetic properties at room temperature. Based on the BET result the specific surface area of nanosheets was evaluated to be $55.1 \text{ m}^2 \text{ g}^{-1}$. Reaction conditions, such as reaction temperature, the volume of hydrazine hydrate, and the different mole ratios of $\text{Co}(\text{NO}_3)_2 \cdot 6\text{H}_2\text{O}$ to Na_2SeO_3 , play an important role for the phase and morphology of the prepared products. The optimal conditions are obtained for the synthesis of the tremelliform $\text{Co}_{0.85}\text{Se}$. The as-prepared $\text{Co}_{0.85}\text{Se}$ nanosheets exhibit excellent catalytic activity and reusability for decomposition of hydrazine hydrate in aqueous solution at room temperature. Therefore, the nonstoichiometric cobalt selenide nanosheets with tremelliform morphology, as a catalyst without noble metal, are expected to remove hydrazine hydrate in wastewater treatment for environmental protection.

Acknowledgment

This work is supported by the National Science Foundation of China (NSFC) (grants 21071002, 20875001, 20871001 and

20905001), Natural Science Foundation of Anhui Province, China (grant no. 11040606M34), the Key Project of Anhui Provincial Education Department (KJ2010A014), financed by the 211 Project of Anhui University, and The Key Laboratory of Environment Friendly Polymer Materials of Anhui Province.

Appendix A. Supplementary data

Supplementary data associated with this article can be found, in the online version, at doi:10.1016/j.apcatb.2012.02.033.

References

- [1] H. Tong, Y.J. Zhu, L.X. Yang, L. Li, L. Zhang, *Angew. Chem. Int. Ed.* 45 (2006) 7739.
- [2] I.U. Arachchige, S.L. Brock, *Acc. Chem. Res.* 40 (2007) 801.
- [3] N.F. Zheng, X.H. Bu, H.W. Lu, L. Chen, P.Y. Feng, *J. Am. Chem. Soc.* 127 (2005) 14990.
- [4] S. Bag, P.N. Trikalitis, P.J. Chupas, G.S. Armatas, M.G. Kanatzidis, *Science* 317 (2007) 490.
- [5] M.V. Kovalenko, M. Scheele, D.V. Talapin, *Science* 324 (2009) 1417.
- [6] S. Bag, M.G. Kanatzidis, *J. Am. Chem. Soc.* 132 (2010) 14951.
- [7] M.R. Gao, S.A. Liu, J. Jiang, C.H. Cui, W.T. Yao, S.H. Yu, *J. Mater. Chem.* 20 (2010) 9355.
- [8] W. Maneepakorn, M.A. Malik, P. O'Brien, *J. Mater. Chem.* 20 (2010) 2329.
- [9] M. Hansen, *Constitution of Binary Alloys*, Geminium Publ. Co., New York, 1985, p. 502.
- [10] X.H. Liu, N. Zhang, R. Yi, G.Z. Qiu, A.G. Yan, H.Y. Wu, D.P. Meng, M.T. Tang, *Mater. Sci. Eng., B* 140 (2007) 38.
- [11] J.H. Zhan, X.G. Yang, S.D. Li, Y. Xie, W.C. Yu, Y. Qian, *J. Solid State Chem.* 152 (2000) 537.
- [12] <http://www.hydrogen.energy.gov/pdfs/progress05/vii.c.8.campbell.pdf>.
- [13] J.F. Zhao, J.M. Song, C.C. Liu, B.H. Liu, H.L. Niu, C.J. Mao, S.Y. Zhang, Y.H. Shen, Z.P. Zhang, *CrystEngComm* 13 (2011) 5681.
- [14] C.E.M. Campos, J.C. de Lima, T.A. Grandi, K.D. Machado, P.S. Pizani, *Chem. Phys. Lett.* 324 (2002) 409.
- [15] P. Nekooi, M. Akbari, M.K. Amini, *Int. J. Hydrogen Energy* 35 (2010) 6392.
- [16] F.Y. Liu, B. Wang, Y.Q. Lai, J. Li, Z.A. Zhang, Y.X. Liu, *J. Electrochem. Soc.* 157 (2010) D523.
- [17] L. Zhu, M. Teo, P.C. Wong, K.C. Wong, I. Narita, F. Ernst, K.A.R. Mitchell, *Appl. Catal., A* 386 (2010) 157.
- [18] Y.J. Feng, T. He, N. Alonso-Vante, *Electrochim. Acta* 54 (2009) 5252.
- [19] A. Besada, *Mikrochim. Acta* 87 (1985) 343.
- [20] R. Kaveeshwar, V.K. Gupta, *Fresenius J. Anal. Chem.* 344 (1992) 114.
- [21] H.W. Schiessl, *Encyclopedia of Chemical Technology*, vol. 12K, Othmer Wiley, New York, 1980, p. 734.
- [22] R. Maurel, J.C. Menezo, *J. Catal.* 51 (1978) 293.
- [23] S.K. Singh, X.B. Zhang, Q. Xu, *J. Am. Chem. Soc.* 131 (2009) 9894.
- [24] X.W. Chen, T. Zhang, M.Y. Zheng, Z.L. Wu, W.C. Wu, C. Li, *J. Catal.* 224 (2004) 473.
- [25] J.B.O. Santos, G.P. Valenca, J.A.J. Rodrigues, *J. Catal.* 210 (2002) 1.
- [26] M.Y. Zheng, X.W. Chen, R.H. Cheng, N. Li, J. Sun, X.D. Wang, T. Zhang, *Catal. Commun.* 7 (2006) 187.
- [27] Y.B. Jang, T.H. Kim, M.H. Sun, J. Lee, S.J. Cho, *Catal. Today* 146 (2009) 196.
- [28] S.K. Singh, Q. Xu, *Chem. Commun.* 46 (2010) 6545.
- [29] S.K. Singh, Q. Xu, *Inorg. Chem.* 49 (2010) 6148.
- [30] L.N. Ding, Y.Y. Shu, A.Q. Wang, M.Y. Zheng, L. Li, X.D. Wang, T. Zhang, *Appl. Catal., A* 385 (2010) 232.
- [31] G.W. Watt, J.D. Chriss, *Anal. Chem.* 24 (1952) 2006.
- [32] F. Cao, R.P. Deng, J.K. Tang, S.Y. Song, Y.Q. Lei, H.J. Zhang, *CrystEngComm* 13 (2011) 223.
- [33] J.M. Song, J.H. Zhu, S.H. Yu, *J. Phys. Chem. B* 110 (2006) 23790.
- [34] A.V. Ananiev, J.C. Broudic, P. Brossard, *Appl. Catal., A* 242 (2003) 1.